Chemistry
A European
Journal

Chemistry Europe
European Chemical Societies Publishing

Accepted Article

Title: The Aggregation Regularity Effect of Multiarylpyrroles on Their Near-Infrared Aggregation-Enhanced Emission Property

Authors: Jiamin Qu, Fei Ren, Jianbing Shi, Bin Tong, Zhengxu Cai, and Yuping Dong

To be cited as: *Chem. Eur. J.* 10.1002/chem.202002525

Link to VoR: https://doi.org/10.1002/chem.202002525

WILEY-VCH

10.1002/chem.202002525

WILEY-VCH

FULL PAPER

The Aggregation Regularity Effect of Multiarylpyrroles on Their Near-Infrared Aggregation-Enhanced Emission Property

Jiamin Qu, Fei Ren, Jianbing Shi,* Bin Tong, Zhengxu Cai and Yuping Dong*

J. Qu, F. Ren, Dr. J. Shi, Prof. B. Tong, Dr. Z. Cai, Prof. Y. Dong
Beijing Key Laboratory of Construction Tailorable Advanced Functional Materialsand Green Applications, School of Materials Science and Engineering
Beijing Institute of Technology
5 South Zhongguancun Str., Haidian District, Beijing 100081, China
E-mail: bing@bit.edu.cn (J. Shi); chdongyp@bit.edu.cn (Y. Dong)

Supporting information for this article is given via a link at the end of the document.

Abstract: Increasing the quantum yield of near-infrared (NIR) emissive dyes is critical for biological applications because these fluorescent dyes generally show decreased emission efficiency under aqueous conditions. In this work, we designed and synthesized several multiarylpyrrole (MAP) derivatives, in which a furanylidene (FE) group at the 3-position of the pyrrole forms donor-π-acceptor molecules, MAP-FE, with a NIR emissive wavelength and aggregation-enhanced emission (AEE) features. Different alkyl chains of MAP-FEs linked to phenyl groups at the 2,5-position of the pyrrole ring resulted in different emissive wavelengths and quantum yields in aggregated states, such as powders or single crystals. Powder XRD data and single crystal analysis elucidated that the different lengths of alkyl chains had a significant impact on the regularity of MAP-FEs when they were forced to aggregate or precipitate, which affected the intermolecular interaction and the restriction degree of the rotating parts, which are essential components. Therefore, an increasing number of NIR dyes could be developed by this design strategy to produce efficient NIR dyes with AEE. Moreover, this method can provide general guidance for other related fields, such as organic solar cells and organic light-emitting materials, because they are all applied in the aggregated state.

Introduction

Near-infrared (NIR) fluorescent dyes have attracted significant attention due to their wide use in many fields, such as biological imaging and tumor treatment, which originates from their deep tissue penetration, reduced background autofluorescence and minimal damage to biological samples.[1-5] However, traditional NIR fluorescent molecules are usually composed of π-conjugated large planar structures, which can emit strong fluorescence in dilute solution but are weakly emissive or even nonfluorescent in the aggregated state. This phenomenon is usually called aggregation-caused quenching (ACQ), which limits their biological applications because most NIR dyes are hydrophobic and prone to aggregation in living organisms. In 2001, Tang's group discovered an intriguing phenomenon: a silole compound, 1-methyl-1,2,3,4,5-pentaphenylsilole, behaved like a weak emitter when dissolved in a good solvent. In contrast, with the addition of poor solvents, aggregates are formed, and the fluorescence intensity gradually increases.[6] This situation is defined as aggregation-induced emission (AIE). In recent years, the discovery of AIE has stimulated the design and preparation of more AIE molecular systems to solve the application problems of traditional fluorescent dyes.[7-10] In addition to the AIE effect, some fluorescent molecules exhibit weak or moderate emission in the single-molecule state, but their emission becomes stronger by the formation of aggregates, showing an aggregation-enhanced emission (AEE) feature.[11-12] AIE/AEE molecules emitting in the NIR region demonstrate "turn on" characteristics in the aggregated state, so the AIE effect promotes the application of NIR dyes in biological fields.[13-16]

At present, through the unremitting efforts of scientists, a large number of NIR AIE/AEE dyes have been developed using electron donor-acceptor (D-A) or donor- π -acceptor (D-π-A) strategies.[17-20] For example, Tang and his coworkers used triphenylamine as a donor and a pyridine salt derivative as an acceptor to synthesize three NIR molecules with targeting effects for synergistic photodynamic therapy, achieving the 1+1+1> 3 effect.[21] Ding's group reported a series of AIE dyes in the NIR region using 2-(4-pyridin-4-ylphenyl) acetonitrile as a receptor and triphenylamine and benzene as donors and then added tetraphenylethylene (TPE) units in the donor part to increase the degree of molecular distortion to reduce intermolecular interactions and to increase reactive oxygen species (ROS) production.[22-23] Ajayaghosh et al. designed a series of diketopyrrolopyrrole-based NIR absorption or emission optoelectronic functional materials by D-A strategy.[24-25] Zhu et al. reported minireviews using a quinoline-malononitrile core as a building block for diversity-oriented synthesis of AIE luminogens (AIEgens).[26] Our group is also devoted to designing AIEgens with long wavelength emission and a high quantum yield in the aggregated state based on multiarylpyrroles (MAPs) as the backbone.[27-30] Among them, AIEgens, with triphenylpyrrole as the conjugate skeleton, triphenylamine as the strong donor, 1-ethyl-3,3-dimethyl-3H-indolium as the strong acceptor and an anchor for the biological target, were synthesized, and the emission wavelength (λ_{em}) reached 724 nm.[30] Moreover, AIEgens can be used for real-time bioimaging of mitochondria under a wash-free staining procedure. Recently, (3-cyano-4,5-dimethyl-2,5-dihydrofuran-2-ylidene) propanedinitrile (FE) was introduced into MAPs as a strong acceptor, and a series of fused-ring groups, such as naphthalene, anthracene, and pyrene, were introduced at the 2,5-position of the pyrrole derivatives to extend the

10.1002/chem.202002525

conjugated skeleton, as shown in Scheme 1. Compounds **MAP1~6-FE** showed AEE properties with NIR emission.[31] However, the introduction of a fused ring group plays a dual role on their emission. One role is an improvement in the quantum yield (QY, Φ_F), and the other role is unfavorable for emission due to the π-π stacking interaction of large planar structures in solids. Therefore, the Φ_F values of these compounds in solids are generally low, and the maximum Φ_F value is 6.56% for maximum emission centered at 679 nm.

With this issue in mind, we further explore how to increase Φ_F in the solid or aggregated state and maximize the AIE advantage of NIR materials.[32-35] Liu et al. optimized the AIE property of NIR molecules by adjusting the length of the alkoxy chain and the position of the substituents. These strategies have been successfully used for image-guided tumor resection.[36] Tang et al. reported that intermolecular rearrangement by increasing the chain length was accelerated to increase the recovery rate from amorphous to crystalline.[37] Li et al. explored the effects of molecular packing and different morphologies on emission behavior.[38-41] Tang and Zhao synthesized a series of pyridinium-functionalized TPE salts that had different alkyl chains. The length of the chain had little influence on the optical properties in solution due to the similar electronic structure, but different hydrophobicities in aqueous media affected the aggregate morphology, leading to diverse emission behaviors.[42] Simple linear alkyl chains play a key role in molecular interactions and packing.[43] Hence, in this work, we introduced alkyl chains of different lengths to the phenyl group at the 2,5-position of pyrrole rings, as shown in Scheme 1, to investigate their NIR emission in the solid state. The FE group was also chosen as an electron acceptor due to its strong electron-withdrawing ability, with 1,2,5-triphenylpyrrole as a donor with a twisting conformation due to its AIE property. Thus, a typical D-π-A structure of MAP-FEs was constructed, and all the obtained compounds exhibited AEE properties, with the maximum emission wavelength up to the NIR region. It is worth mentioning that the synthesized compounds had higher QYs in the solid state in the NIR range. More importantly, different alkyl chain lengths resulted in different regular packing, which affected their QY in the aggregated state, as shown through techniques such as powder X-ray diffraction (XRD) and single crystals.

Results and Discussion

Design and Synthesis. According to our previous work, the phenyl ring at the 2,5-position of pyrrole can increase the conjugation degree of the dye skeleton,[44] the FE group is a strong electron-withdrawing group, and p-benzoate ethyl ester group at the 1-position of the pyrrole can be easily post-functionalized into other functional or biological target group when necessary.[31] Therefore, the aim of introducing alkyl chains on the phenyl ring located at the 2,5-position of pyrrole is mainly to explore their effect on the molecular packing regularity in the aggregated state, particularly in the solid state. The detailed synthetic routes for **MAP7~12-FE** are shown in Scheme S1 of the Supporting Information (SI), and the chemical structures of all the compounds, including the intermediates and the target dyes, were confirmed by nuclear magnetic resonance (NMR) spectroscopy and mass spectroscopy (MS), the results of which are also shown in Figures S1~S52. In addition, **MAP7~12-FE** have better solubility in polar organic solvents, such as tetrahydrofuran (THF) and dimethyl sulfoxide (DMSO).

Photophysical Properties in Solution and Solid. The UV-vis absorption spectra of MAP-FEs were collected in THF solution and are shown in Figure 1a. All the compounds, MAP7~12-FE,

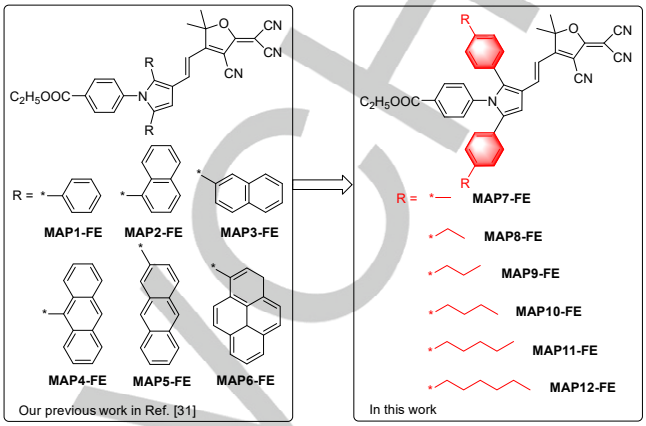

Scheme 1. Structures of MAP-FEs used in our previous work and in this work.

demonstrated similar absorption bands and had strong absorption in the visible region from 400 to 600 nm. Even the aggregates of MAP-FEs in the mixed solution of THF as a good solvent and H_2O as a poor solvent with a 90% water fraction (f_w) also showed similar absorption behavior, as illustrated in Figure 1b. These results indicated that the length of the alkyl side chain of the phenyl ring linked at the 2,5-position of pyrrole had little effect on the UV-vis absorption spectra of MAP-FEs in solution.

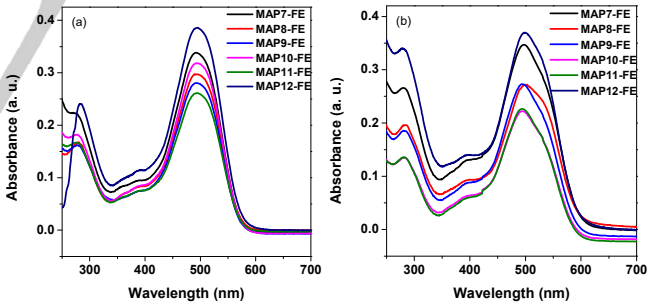

Figure 1. (a) Absorption spectra of MAP-FEs in THF. (b) Absorption spectra of MAP-FEs in the mixture of THF/H_2O with a 90% water fraction. [MAP-FEs] = 1.0 × 10^{-5} mol/L.

Next, the normalized photoluminescence (PL) spectra of MAP-FEs in THF and in solid were obtained and are shown in Figure 2. **MAP7~12-FE** showed the same emission behaviors in THF, such as maximum peak wavelengths (λ_{em}) at 622 nm and a full width at half maximum (FWHM) of 100 nm (Figure 2a). However, they showed different λ_{em} values in powder as an aggregated state ranging from 636 to 683 nm, as shown in Figure 2b. The FWHM of **MAP7~12-FE** narrowed to 64, 83, 81, 66, 85, and 87 nm, respectively. Moreover, the λ_{em} increased in sequence with the increasing length of alkyl chains, except **MAP7-FE**. The unusual λ_{em} of **MAP7-FE** will be discussed in the following single crystal

10.1002/chem.202002525

section. All these results indicated that the length of the alkyl chain of the phenyl ring linked at the 2,5-position of pyrrole had an obvious effect on the PL property of MAP-FEs in the solid state, which clarified their aggregation behavior as the target dyes.

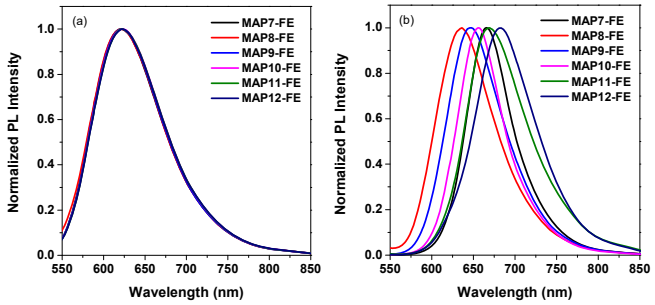

Figure 2. (a) Normalized PL spectra of MAP-FEs in THF. (b) Normalized PL spectra of MAP-FEs in powder. Excited wavelength (λ_{ex}): 510 nm for THF solution and 500 nm for powder state; [MAP-FEs] = 1.0 × 10^{-5} mol/L.

The AEE Characteristics with NIR Emission. As mentioned above, both the λ_{em} and FWHM were different among these MAP-FEs in the solid state. Therefore, their aggregated PL spectra were obtained by changing the poor solvent of the water fraction f_w, and the results are shown in Figure S53. In a pure THF solution of 1.0 × 10^{-5} mol/L, the MAP-FEs showed a certain emissive intensity, which means that all these dyes could emit in dilute solution. Then, the fluorescence became weak when a small amount of water was added into the THF solution, which showed a typical solvent effect of fluorescent dyes in polar solvents. However, further increasing f_w resulted in a fluorescence increase after f_w up to 60% or 70%, and the PL intensity reached a maximum at f_w = 90%, showing AEE characteristics.

Further, other photophysical data, including Φ_F and the fluorescence lifetime (τ) in solution and in the solid state, are summarized in Table 1. Moreover, the radiative transition rate constant (k_r) and nonradiative transition rate constant (k_{nr}) could be obtained from Φ_F and τ according to the equations $\Phi_F = k_r/(k_r+k_{nr})$ and $\tau = 1/(k_r+k_{nr})$, respectively.[45] There is almost no difference in the QYs and lifetimes of the MAP-FEs in THF. The value of k_{nr} is approximately two orders of magnitude higher than that of k_r, which leads to a low Φ_F due to the freely rotating phenyl groups as rotors in these NIR dyes, which largely dissipate the radiation energy via a thermal/kinetic energy loss. Both Φ_F and τ increased for the solid of MAP-FEs that were compactly aggregated. The value of k_{nr} was greatly decreased, while that of k_r showed almost no obvious change; thus, the NIR emission intensities of all the MAP-FEs in the solid state greatly increased. That is, the mechanism of AEE typically belongs to the restricted intramolecular rotation (RIR) effect, which is affiliated with restricted intramolecular motion (RIM). However, it is worth noting that the six NIR dyes exhibited significant differences among their Φ_Fs collected from their powder samples. The values of Φ_F were 19.38%, 25.82%, 15.00%, 32.86%, 14.62% and 7.07% for **MAP7-FE** to **MAP12-FE** in the solid state, respectively. Considering the same skeleton structure of these NIR dyes, the solid-state emission efficiency is much different and must be related to the length of the alkyl chain. The longer alkyl chain resulted in the looser compactness in solid. So the RIR degree of MAP12-FE is less than others and the quantum yield in solid powder is lowest. To sufficiently confirm that the length of the alkyl chain has a greater effect on the emission behavior of MAP-FEs in the aggregated state, such as solid powders, an immobilized single-molecule state of all the MAP-FEs was prepared by dispersing the dye molecules into polymethyl methacrylate (PMMA) films, which can lock the rotation of the phenyl rings of pyrroles. The QYs of the MAP-FEs in PMMA films exhibited little difference, as shown in Table 1, which in turn, verified that the length of the alkyl chain can affect the compaction degree in the aggregated state of these MAP-FEs when they were forced to aggregate. In addition, density functional theory (DFT) was used to calculate the energy levels of the MAP-FEs in the single-molecule state by Gaussian 09 (Figure S54). The results of the DFT calculation demonstrated that the orbital energy level of the highest occupied molecular orbital (HOMO) and lowest unoccupied molecular orbital (LUMO) hardly changed with the length of the alkyl chain, which was consistent with the experimental photophysical results of these NIR dyes in solution and in PMMA films. In other words, the length of the alkyl chain on the phenyl ring has a profound impact on their NIR emissive properties of MAP-FEs in the aggregated state, such as powders or crystals. All the above results indicated that the AEE feature authentically originated the reduced nonradiative energy loss due to RIR and that the regularity/compactness of NIR dyes had an important effect on the AEE efficiency.

Next, the effect of the length of the alkyl chain on the phenyl rings of the MAP-FEs on their NIR emissive efficiency was investigated by powder X-ray diffraction (PXRD). The pristine samples that were obtained by removing the solvent from the

Table 1. Summary of the photophysical data for the MAP-FEs in solution, in the solid state and in PMMA films.

Compounds	Solution[a]						Solid						PMMA film[d]		
	λ_{ex}[b] (nm)	λ_{em} (nm)	Φ_F (%)	τ[c] (ns)	k_r (×10^8 s^{-1})	k_{nr} (×10^8 s^{-1})	λ_{ex}[b] (nm)	λ_{em} (nm)	Φ_F (%)	τ[c] (ns)	k_r (×10^8 s^{-1})	k_{nr} (×10^8 s^{-1})	λ_{ex}[b] (nm)	λ_{em} (nm)	Φ_F (%)
MAP7-FE	510	621	1.50	0.24	0.6250	41.04	490	668	19.38	3.51	0.5521	2.297	470	626	27.93
MAP8-FE	516	621	1.49	0.48	0.3104	20.52	515	645	25.82	3.52	0.7335	2.107	515	632	34.18
MAP9-FE	510	622	1.72	0.25	0.6880	39.31	502	647	15.00	2.88	0.5208	2.951	470	625	30.91
MAP10-FE	511	623	1.56	0.24	0.6500	41.02	504	663	32.86	5.30	0.6200	1.267	475	623	36.45
MAP11-FE	510	623	1.61	0.47	0.3426	20.93	503	672	14.62	1.94	0.7536	4.401	510	618	37.11
MAP12-FE	505	623	1.64	0.16	1.0250	61.48	500	682	7.07	3.17	0.2303	2.924	510	613	37.89

Notes: [a] Measured in THF at [MAP-FEs] = 1.0 × 10^{-5} mol/L. [b] The excitation wavelength (λ_{ex}) for obtaining the absolute fluorescence quantum yield (Φ_F) was determined by integrating a sphere. [c] An average lifetime. [d] The PMMA film is made from PMMA solution containing 0.5 *wt*% MAP-FEs and then dried in vacuum.

10.1002/chem.202002525

rotary evaporation apparatus during the purifying process and by embedding dyes into PMMA were used for PXRD characterization. As shown in Figure 3a, the PXRD pattern of **MAP10-FE** showed strong and sharp diffraction peaks, which means that it had good regularity when forcing dye molecules to precipitate from solution. This result can well explain why the abovementioned QY of **MAP10-FE** in powder (32.86%) was higher than others. The more compact the state is, the more restricted it is. The good regularity of **MAP10-FE** is well self-assembled when precipitating, which is very favorable to AEE. Therefore, on the other hand, the length of the alkyl chain on the rotating part had significant effects on the AEE behaviors if the dyes were arranged spontaneously. Different alkyl chain lengths cause different spontaneous arrangement degrees. The relatively good QY of **MAP8-FE** (25.82%) also corresponded to a relatively good regularity since relatively sharp peaks appeared. When 0.5*wt*% of the MAP-FEs was doped into a pure PMMA solution and then prepared for thin films, all the sharp peaks disappeared, as shown in Figure 3b, because the molecules of the MAP-FEs were frozen into PMMA, making it difficult for them to effectively

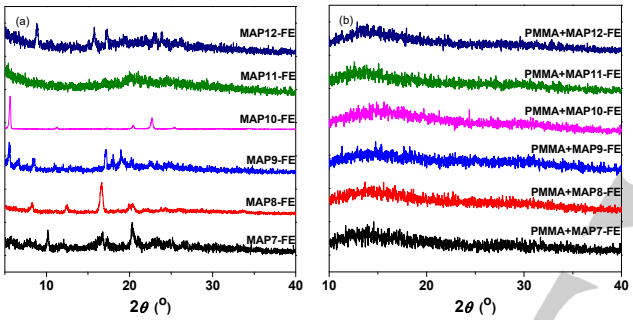

Figure 3. (a) XRD data of the MAP-FEs in pristine powder. (b) XRD data of MAP-FEs in homodisperse PMMA films.

self-arrange. This result is highly consistent with their QYs listed in Table 1; little difference was observed for frozen molecules. This strategy for regulating the length of the side chains on the rotating parts provides an ideal and feasible way to design highly efficient NIR molecules with narrow FWHMs in the aggregated state.

Lastly, single crystals of the MAP-FEs were obtained by slowly evaporating a mixture of dichloromethane and petroleum ether. The molecular structures of **MAP9-FE** and **MAP10-FE** in single crystals, as an example for a related discussion, are shown in Figure 4. The twist angles between the pyrrole ring and other ring substituents at the 1, 2, 3, and 5-positions are illustrated in Figures 4a and 4e. The relatively large twisting angles between the pyrrole ring and the phenyl ring at the 1,2,5-position of pyrrole ensured the higher emission efficiency in the solid due to reducing the π-π stacking interaction that caused ACQ. The very small twisting angles between the pyrrole ring and the FE group at the 3-position of pyrrole through the vinylidene group spacer benefited the electron transfer among D-π-A when excited, which was favorable to narrow the energy gap and to red-shift the emission wavelength. Single crystals of **MAP7-FE**, **MAP8-FE**, **MAP11-FE**, and **MAP12-FE** showed similar twisting angles, as shown in Figure S55. It is also worth noting that the twisting angle of the FE group of **MAP7-FE** and the pyrrole ring was only 2.5° (Figure S55a), which was a probable cause for its irregular λ_{em} (see Figure 2b) compared with the other NIR dyes. In addition, the C-H···π interaction of **MAP9-FE** and **MAP10-FE** was found to have close distances of 2.686 Å and 2.788 Å, respectively, as shown in Figures 4b and 4f, which can effectively restrict intramolecular motion and then block the nonradiative energy decay channel, thus promoting the AEE efficiency of solid MAP-FEs in the NIR region. Moreover, there are also hydrogen bonding interactions, such as the C-H···O and C-H···N interactions, in **MAP9-FE** and **MAP10-FE**, as shown in Figures 5c, 5d, and 5g-5i, and all these intermolecular interactions had a positive effect on their AEE efficiency. Similar interactions of C-H···π and hydrogen bonding were observed in other length of alkyl chains of **MAP7-FE, MAP8-FE, MAP11-FE** and **MAP12-FE**. The only difference was that **MAP10-FE**, which has an n-butyl on the phenyl ring located at the 2,5-position of pyrrole, had more intermolecular interactions than others, which is beneficial to closer packing when the molecules are constrainedly arranged from the single molecular state to the solid state. This is a critical cause of the better emission efficiency of **MAP10-FE** in the solid state. Therefore, according to the single crystal analysis, designing NIR emissive dyes in the aggregated state should fortify multiple intermolecular interactions but avoid π-π stacking through introduction of some alkyl chains in the rotating segments.

Thermal analysis. The difference in the single crystals of the

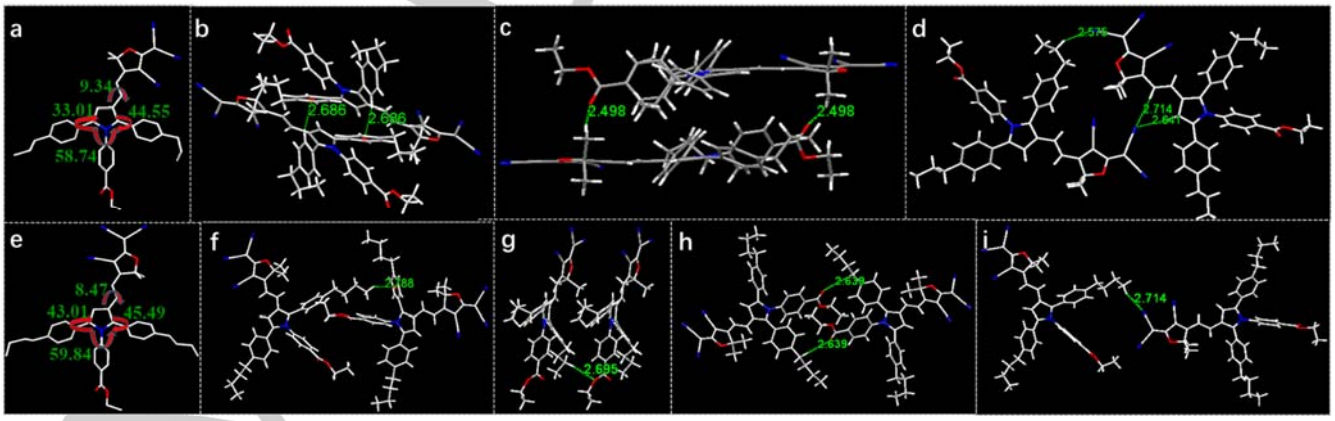

Figure 4. Molecular structure of (a) **MAP9-FE** (CDCC:1936113) and (e) **MAP10-FE** (CDCC:1987059). C-H···π interactions between the adjacent molecules in the single crystal of (b) **MAP9-FE** and (f) **MAP10-FE**. C-H···O interactions between the adjacent molecules of (c) **MAP9-FE** and (g and h) **MAP10-FE**. C-H···N interactions between the adjacent molecules of (d) **MAP9-FE** and (i) **MAP10-FE**.

10.1002/chem.202002525

MAP-FEs motivated us to further explore the effects of alkyl chains on their thermodynamic properties, such as the melting point, thermal decomposition temperature, and exothermic heat. Therefore, thermogravimetric analysis (TGA) and differential scanning calorimetry (DSC) were carried out, and the corresponding graphs are shown in Figures 5 and S56. The temperature to reach a 5% weight loss for all the dyes was higher than 340 °C, as shown in Figure 5a, which showed good thermal stability. However, the DSC curves in heating or cooling showed different thermal behaviors, as shown in Figures 5b and S56. The melting point showed the same value in the first heating and the second heating. The values of the melting points were 292, 275, 243, 217, 179 and 170 °C for **MAP7~12-FE**, respectively. Additionally, there was a certain proportionality between the melting point and the length of alkyl chains, as described in Figure S57; the melting point of MAP-FEs gradually decreased with the extension of the alkyl chains. A different compact degree resulted in different melting points due to different alkyl chains.

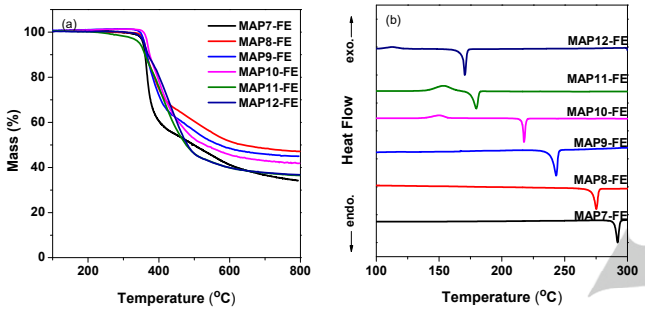

Figure 5. (a) TGA graphs of MAP-FEs. (b) DSC curves for the secondary heating of MAP-FEs. The heating rate is 10 K/min under N_2.

Conclusion

In summary, six NIR MAP-FEs with AEE properties were synthesized, and their photophysical properties were observed in different molecular states, especially in solid state. Introducing alkyl chains with different lengths on the benzene ring at the 2,5-position of the pyrrole ring had important effects on the NIR emissive efficiency of the MAP-FEs. The results, as confirmed by PXRD and single crystal analysis, indicated that the length of the alkyl chain mainly affected the regularity of the aggregated state, which further led to more intermolecular interactions for the suitable length and restrained the nonradiative energy loss and thus changed their Φ_F. Additionally, the smaller dihedral angle between the electron acceptor FE group and the electron donor pyrrole ring facilitated the red shift of the emission wavelength. All these results provide theoretical and experimental support for designing and developing other excellent NIR organic dyes with AEE characteristics.

Experimental Section

Materials and equipment

The synthesis process is shown in Scheme S1, all compounds were used without further purification. $Pd(PPh_3)_4$ was purchased from J&K, $POCl_3$ was purchased from Xiya Reagent. K_2CO_3, CH_3COONH_4 and chloroform-*d* were purchased from Innochem. 4-methylphenylboronic acid, 4-ethylphenylboronic acid, 4-propylphenylboronic acid, 4-butylphenylboronic acid, 4-pentylphenylboronic acid and 4-hexyl phenylboric acid were all purchased from Sukailu.

^1H and ^{13}C NMR spectra were recorded on a Bruker AV 400 spectrometer. Mass spectra were measured by using a Finnigan Biflex III mass spectrometer. UV/Vis absorption spectra were recorded on a TU-1901 UV/Vis spectrophotometer. Photoluminescence spectra were recorded on a Hitachi F-7000 spectrophotometer. PL quantum yields were measured by using an integrating sphere on a NanoLog FL3-2iHR fluorescence spectrometer (Horiba Jobin Yvon), and PL time-resolved decays were measured with a DeltaFlex ultrafast lifetime spectrofluorometer (Horiba Jobin Yvon). Single-crystal data were collected on a Bruker-AXS SMART APEX 2 CCD diffractometer. TG data were measured on a TGA/DSC3+ thermal analyzer. DSC data were measured on a DSC3+ thermal analyzer. The XRD patterns were measured by an X'Pert Pro MRD X-ray single crystal diffractometer.

Synthesis of compounds MAP7~12-FE

The synthesis method of compounds ethyl 4-(2,5-dibromo-1*H*-pyrrol-1-yl)benzoate and 2-(3-cyano-4,5,5-trimethylfuran-2(5H)-ylidene)malononitrile has been reported.[31] The synthesis steps of intermediates **MAP7~12** and **MAP7~12-CHO** are detailed in Supporting Information(SI). Specific synthesis methods of target compounds **MAP7~12-FE** are given below.

Synthesis of MAP-FEs: MAP-CHOs (0.50 mmol), 2-(3-cyano-4,5,5-trimethylfuran-2(5H)-ylidene)malononitrile (0.1905 g, 0.55 mmol) and CH_3COONH_4 (0.0425 g, 0.55 mmol) were dissolved in 10 mL THF/C_2H_5OH (4/1) mixed solvents and then stirred at room temperature for 24 h. The solvent was evaporated under reduced pressure and the residue was purified by silica gel column chromatography using a dichloromethane/petroleum ether mixture (1/3, V_d/V_p) as the eluent to give desired compound **MAP-FEs** with a certain yield.

MAP7-FE: The yield gives 75.9%. ^1H NMR (400 MHz, $CDCl_3$): δ = 7.90 (d, *J* = 8.4 Hz, 2H), 7.65 (d, *J* = 15.6 Hz, 1H), 7.12 (d, *J* = 7.6 Hz, 2H), 7.07-6.93 (m, 8H), 6.86 (s, 1H), 6.74 (d, *J* = 15.6 Hz, 1H), 4.35 (q, *J* = 7.2 Hz, 2H), 2.33 (d, *J* = 15.6 Hz, 6H), 1.63 (s, 6H), 1.37 (t, *J* = 7.2 Hz, 3H). ^{13}C NMR (100 MHz, $CDCl_3$): δ = 176.20, 174.98, 165.58, 143.05, 142.84, 141.18, 139.33, 138.71, 138.01, 130.52, 130.28, 129.98, 129.42, 129.15, 128.72, 128.33, 127.83, 125.88, 121.37, 112.46, 111.66, 111.10, 110.95, 106.71, 96.88, 95.09, 61.42, 55.24, 26.55, 21.37, 21.21, 14.26. HR-MS (APCI, *m/z*) Calcd for $C_{39}H_{32}N_4O_3$ $[M+H]^+$: 605.2547, found: 605.2568, error 3.37 ppm.

MAP8-FE: The yield gives 44.9%. ^1H NMR (400 MHz, $CDCl_3$): δ = 7.91 (d, *J* = 8.8 Hz, 2H), 7.65 (d, *J* = 16.0 Hz, 1H), 7.15 (d, *J* = 8.0 Hz, 2H), 7.12-6.92 (m, 8H), 6.86 (s, 1H), 6.74 (d, *J* = 16.0 Hz, 1H), 4.36 (q, *J* = 7.2 Hz, 2H), 2.74-2.53 (m, 4H), 1.62 (s, 6H), 1.37 (t, *J* = 7.2 Hz, 3H), 1.27 (q, *J* = 7.6 Hz, 6H). ^{13}C NMR (100 MHz, $CDCl_3$): δ = 176.25, 175.03, 165.64, 145.50, 144.25, 143.14, 142.98, 141.23, 138.76, 130.61, 130.29, 130.00, 128.77, 128.37, 128.16, 128.06, 127.94, 126.11, 121.45, 112.50, 111.70, 111.11, 110.96, 106.81, 96.92, 95.03, 61.43, 55.15, 28.55, 28.50, 26.53, 15.19, 15.01, 14.28. HR-MS (APCI, m/z) Calcd for $C_{41}H_{36}N_4O_3$ $[M+H]^+$: 633.2860, found: 633.2850, error -1.65 ppm.

MAP9-FE: The yield gives 62.4%. ^1H NMR (400 MHz, $CDCl_3$): δ = 7.90 (d, *J* = 8.4 Hz, 2H), 7.63 (d, *J* = 16.0 Hz, 1H), 7.13 (d, *J* = 8.4 Hz, 2H), 7.10-6.90 (m, 8H), 6.86 (s, 1H), 6.74 (d, *J* = 16.0 Hz, 1H), 4.36 (q, *J* = 7.2 Hz, 2H), 2.65-2.48 (m, 4H), 1.69-1.56 (m, 10H), 1.37 (t, *J* = 7.2 Hz, 3H), 1.01-0.84 (m, 6H). ^{13}C NMR (100 MHz, $CDCl_3$): δ = 176.20, 174.97, 165.62, 144.05, 143.12, 142.93, 142.78, 141.21, 138.75, 130.53, 130.24, 129.99, 128.74, 128.68, 128.52, 128.32, 128.06, 126.16, 121.44, 112.47, 111.66, 111.06, 110.94, 106.77, 96.85, 95.13, 61.41, 55.25, 37.68, 26.53, 24.42,

24.25, 24.12, 14.27, 13.81, 13.71. HR-MS (APCI, *m/z*) Calcd for $C_{43}H_{40}N_4O_3$ [M+H]$^+$: 661.3173, found: 661.3194, error 3.11 ppm.

MAP10-FE: The yield gives 50.4%. ^{1}H NMR (400 MHz, $CDCl_3$): δ = 7.92 (d, *J* = 8.4 Hz, 2H), 7.65 (d, *J* = 16.0 Hz, 1H), 7.16 (d, *J* = 8.0 Hz, 2H), 7.11-6.95 (m, 8H), 6.88 (s, 1H), 6.76 (d, *J* = 15.6 Hz, 1H), 4.38 (q, *J* = 7.2 Hz, 2H), 2.68-2.54 (m, 4H), 1.64 (s, 6H), 1.62-1.56 (m, 4H), 1.42-1.31 (m, 7H), 0.99-0.92 (m, 6H). ^{13}C NMR (100 MHz, $CDCl_3$): δ = 176.23, 175.02, 165.63, 144.28, 143.18, 143.01, 142.98, 141.21, 138.76, 130.55, 130.26, 129.98, 128.70, 128.47, 128.33, 128.01, 126.10, 121.45, 112.51, 111.70, 111.09, 110.94, 106.76, 96.89, 95.08, 61.42, 55.17, 35.36, 35.32, 33.32, 33.12, 26.54, 22.39, 22.34, 14.27, 13.94. HR-MS (APCI, *m/z*) Calcd for $C_{45}H_{44}N_4O_3$ [M]$^+$: 688.3408, found: 688.3398, error -1.47 ppm.

MAP11-FE: The yield gives 46.0%. ^{1}H NMR (400 MHz, $CDCl_3$): δ = 7.92 (d, *J* = 8.4 Hz, 2H), 7.64 (d, *J* = 15.6 Hz, 1H), 7.16 (d, *J* = 8.0 Hz, 2H), 7.13-6.92 (m, 8H), 6.88 (s, 1H), 6.77 (d, *J* = 16.0 Hz, 1H), 4.38 (q, *J* = 7.2 Hz, 2H), 2.69-2.52 (m, 4H), 1.64 (s, 6H), 1.67-1.56 (m, 10H), 1.46-1.20 (m, 11H), 1.00-0.82 (m, 6H). ^{13}C NMR (100 MHz, $CDCl_3$): δ = 176.21, 175.00, 165.62, 144.30, 143.16, 143.04, 142.95, 141.21, 138.76, 130.55, 130.25, 129.98, 128.70, 128.47, 128.33, 128.01, 126.11, 121.44, 112.50, 111.68, 111.08, 110.96, 106.75, 96.87, 95.13, 61.41, 55.20, 35.61, 31.51, 31.43, 30.84, 30.63, 26.55, 22.51, 22.48, 14.27, 14.08, 14.05. HR-MS (APCI, *m/z*) Calcd for $C_{47}H_{48}N_4O_3$ [M+H]$^+$: 717.3799, found: 717.3792, error -1.07 ppm.

MAP12-FE: The yield gives 47.5%. ^{1}H NMR (400 MHz, $CDCl_3$): δ = 7.89 (d, *J* = 8.4 Hz, 2H), 7.62 (d, *J* = 15.6 Hz, 1H), 7.13 (d, *J* = 7.6 Hz, 2H), 7.09-6.89 (m, 8H), 6.86 (s, 1H), 6.74 (d, *J* = 16.0 Hz, 1H), 4.35 (q, *J* = 7.2 Hz, 2H), 2.68-2.47 (m, 4H), 1.63-1.54 (m, 10H), 1.37 (t, *J* = 7.2 Hz, 3H), 1.31-1.25 (m, 12H), 0.92-0.83 (m, 6H). ^{13}C NMR (100 MHz, $CDCl_3$): δ = 176.20, 174.98, 165.62, 144.30, 143.13, 143.05, 142.92, 141.22, 138.77, 130.54, 130.24, 129.98, 128.70, 128.46, 128.33, 128.01, 126.11, 121.43, 112.48, 111.66, 111.06, 110.97, 106.76, 96.85, 95.16, 61.41, 55.23, 35.64, 31.65, 31.60, 31.10, 30.89, 28.94, 28.85, 26.55, 22.59, 14.26, 14.06. HR-MS (APCI, *m/z*) Calcd for $C_{49}H_{52}N_4O_3$ [M-H]$^+$: 743.3967, found: 743.3962, error -0.57 ppm.

Acknowledgements

This work was financially supported by the National Natural Science Foundation of China (Nos. 21875019, 51673024, 21975020 and 51803009), the National Key Research and Development Program of China (No. 2018YFA0901800) and Beijing Institute of Technology Research Fund Program for Young Scholars.

Keywords: near-infrared emission • aggregation-enhanced emission • multiarylpyrrole • alkyl chain length • restricted intramolecular rotation

[1] Z. Zheng, D. Li, Z. Liu, H. Q. Peng, H. H. Y. Sung, R. T. K. Kwok, I. D. Williams, J. W. Y. Lam, J. Qian, B. Z. Tang, *Adv. Mater.* **2019**, *31,* 1904799.

[2] B. Braun, I. Wehl, D. K. Kolmel, U. Schepers, S. Brase, *Chem. Eur. J.* **2019**, *25*, 7998-8002.

[3] W. Qin, N. Alifu, Y. Cai, J. W. Y. Lam, X. He, H. Su, P. Zhang, J. Qian, B. Z. Tang, *Chem. Commun.* **2019**, *55*, 5615-5618.

[4] Z. Zheng, H. Liu, S. Zhai, H. Zhang, G. Shan, R. T. K. Kwok, C. Ma, H. H. Y. Sung, I. D. Williams, J. W. Y. Lam, K. S. Wong, X. Hu, B. Z. Tang, *Chem. Sci.* **2020**, *11*, 2494-2503.

[5] M. Dai, H. Lee, Y. J. Yang, M. Santra, C. W. Song, Y. W. Jun, Y. J. Reo, W. J. Kim, K. H. Ahn, *Chem. Eur. J.* **2020**, DOI: 10.1002/chem.202001163.

[6] J. Luo, Z. Xie, J. W. Lam, L. Cheng, H. Chen, C. Qiu, H. S. Kwok, X. Zhan, Y. Liu, D. Zhu, B. Z. Tang, *Chem. Commun.* 2001, 1740-1741.

[7] Y.-L. Wang, C. Fan, B. Xin, J.-P. Zhang, T. Luo, Z.-Q. Chen, Q.-Y. Zhou, Q. Yu, X.-N. Li, Z.-L. Huang, C. Li, M.-Q. Zhu, B. Z. Tang, *Mater. Chem. Front.* **2018**, *2*, 1554-1562.

[8] X. Cai, B. Liu, *Angew. Chem. Int. Ed.* **2020**, DOI: 10.1002/anie.202000845.

[9] Y. Zhang, H. Xu, W. Xu, C. Zhang, J. Shi, B. Tong, Z. Cai, Y. Dong, *Sci. Chi. Chem.* **2019**, *62*, 1393-1397.

[10] R. Thirumalai, R. D. Mukhopadhyay, V. K. Praveen, A. Ajayaghosh, *Sci. Rep.* **2015**, *5*, 9842.

[11] X. Yang, Q. Wang, P. Hu, C. Xu, W. Guo, Z. Wang, Z. Mao, Z. Yang, C. Liu, G. Shi, L. Chen, B. Xu, Z. Chi, *Mater. Chem. Front.* **2020**, *4*, 941-949.

[12] J. Yang, Z. Chi, W. Zhu, B. Z. Tang, Z. Li, *Sci. Chi. Chem.* **2019**, *62*, 1090-1098.

[13] J. S. Ni, P. Zhang, T. Jiang, Y. Chen, H. Su, D. Wang, Z. Q. Yu, R. T. K. Kwok, Z. Zhao, J. W. Y. Lam, B. Z. Tang, *Adv. Mater.* **2018**, *30*, e1805220.

[14] M. Gao, F. Yu, C. Lv, J. Choo, L. Chen, *Chem. Soc. Rev.* **2017**, *46*, 2237-2271.

[15] X. Ge, M. Gao, B. Situ, W. Feng, B. He, X. He, S. Li, Z. Ou, Y. Zhong, Y. Lin, X. Ye, X. Hu, B. Z. Tang, L. Zheng, *Mater. Chem. Front.* **2020**, *4*, 957-964.

[16] T. Xue, X. Jia, J. Wang, J. Xiang, W. Wang, J. Du, Y. He, *Chem. Eur. J.* **2019**, *25*, 9634-9638.

[17] Q. Zhao, J. Z. Sun, *J. Mater. Chem. C.* **2016**, *4*, 10588-10609.

[18] J. Merz, M. Dietz, Y. Vonhausen, F. Wöber, A. Friedrich, D. Sieh, I. Krummenacher, H. Braunschweig, M. Moos, M. Holzapfel, C. Lambert, T. B. Marder, *Chem. Eur. J.* **2019**, *26*, 438-453.

[19] D. G. Congrave, B. H. Drummond, P. J. Conaghan, H. Francis, S. T. E. Jones, C. P. Grey, N. C. Greenham, D. Credgington, H. Bronstein, *J. Am. Chem. Soc.* **2019**, *141*, 18390-18394.

[20] S. Cherumukkil, S. Ghosh, V. K. Praveen, A. Ajayaghosh, *Chem. Sci.* **2017**, *8*, 5644-5649.

[21] W. Xu, M. M. S. Lee, J. J. Nie, Z. Zhang, R. T. K. Kwok, J. W. Y. Lam, F. J. Xu, D. Wang, B. Z. Tang, *Angew. Chem. Int. Ed.* **2020**, DOI: 10.1002/anie.202000740.

[22] C. Chen, X. Ni, S. Jia, Y. Liang, X. Wu, D. Kong, D. Ding, *Adv. Mater.* **2019**, *31*, e1904914.

[23] C. Chen, X. Ni, H. W. Tian, Q. Liu, D. S. Guo, D. Ding, *Angew. Chem. Int. Ed.* **2020**, DOI: 10.1002/anie.201916430.

[24] S. Ghosh, R. Raveendran, A. Saeki, S. Seki, M. Namboothiry, A. Ajayaghosh, *ACS Appl. Mater. Interfaces* **2019**, *11*, 1088-1095.

[25] S. Ghosh, S. Shankar, D. S. Philips, A. Ajayaghosh, *Mater. Today Chem.* **2020**, *16,* 100242.

[26] Z. Guo, C. Yan, W.-H. Zhu, *Angew. Chem. Int. Ed.* **2020**, DOI: 10.1002/anie.201913249.

[27] Y. Lei, W. Dai, Z. Liu, S. Guo, Z. Cai, J. Shi, X. Zheng, J. Zhi, B. Tong and Y. Dong, *Mater. Chem. Front.* **2019**, 3, 284-291.

[28] Y. Li, Y. Lei, L. Dong, L. Zhang, J. Zhi, J. Shi, B. Tong, Y. Dong, *Chem. Eur. J.* **2019**, *25*, 573-581.

[29] P. Liu, W. Li, S. Guo, D. Xu, M. Wang, J. Shi, Z. Cai, B. Tong, Y. Dong, *ACS Appl. Mater. Interfaces* **2018**, 10, 23667-23673.

[30] F. Ren, P. Liu, Y. Gao, J. Shi, B. Tong, Z. Cai, Y. Dong, *Mater. Chem. Front.* **2019**, *3*, 57-63.

[31] F. Ren, J. Shi, B. Tong, Z. Cai, Y. Dong, *Mater. Chem. Front.* **2019**, *3*, 2072-2076.

[32] J. Yang, Z. Ren, B. Chen, M. Fang, Z. Zhao, B. Z. Tang, Q. Peng, Z. Li, *J. Mater. Chem. C.* **2017**, *5*, 9242-9246.

[33] Q. Wang, B. Xia, J. Xu, X. Niu, J. Cai, Q. Shen, W. Wang, W. Huang, Q. Fan, *Mater. Chem. Front.* **2019**, *3*, 650-655.

[34] J.-Y. Zhu, C.-X. Li, P.-Z. Chen, Z. Ma, B. Zou, L.-Y. Niu, G. Cui, Q.-Z. Yang, *Mater. Chem. Front.* **2020**, *4*, 176-181.

[35] J. Zhu, J. Zou, Z. Zhang, J. Zhang, Y. Sun, X. Dong, Q. Zhang, *Mater. Chem. Front.* **2019**, *3*, 1523-1531.

[36] J. Liu, C. Chen, S. Ji, Q. Liu, D. Ding, D. Zhao, B. Liu, *Chem. Sci.* **2017**, *8*, 2782-2789.

[37] Y. Dong, J. Zhang, A. Li, J. Gong, B. He, S. Xu, J. Yin, S. H. Liu, B. Z. Tang, *J. Mater. Chem. C.* **2020**, *8*, 894-899.

[38] C. Wang, Z. Li, *Mater. Chem. Front.* **2017**, *1*, 2174-2194.

10.1002/chem.202002525

[39] C. Wang, Y. Yu, Z. Chai, F. He, C. Wu, Y. Gong, M. Han, Q. Li, Z. Li, *Mater. Chem. Front.* **2019**, *3*, 32-38.
[40] J. Wang, Z. Chai, J. Wang, C. Wang, M. Han, Q. Liao, A. Huang, P. Lin, C. Li, Q. Li, Z. Li, *Angew. Chem. Int. Ed.* **2019**, *58*, 17297-17302.
[41] Q. Li, Z. Li, *Acc. Chem. Res.* **2020**, *53*, 962-973.
[42] N. Li, Y. Y. Liu, Y. Li, J. B. Zhuang, R. R. Cui, Q. Gong, N. Zhao, B. Z. Tang, *ACS Appl. Mater. Interfaces* **2018**, *10*, 24249-24257.
[43] Z. Qiu, Z. Yang, W.-C. Chen, L. Xing, S. Hu, S. Ji, Q. Yang, N. Cai, X. Ouyang, Y. Huo, *J. Mater. Chem. C.* **2020**, *8*, 4139-4147.
[44] Y. Lei, Q. Liu, L. Dong, Z. Cai, J. Shi, J. Zhi, B. Tong, Y. Dong, *Chem. Eur. J.* **2018**, *24*, 14269-14274.
[45] J. Shi, Y. Wu, S. Sun, B. Tong, J. Zhi, Y. Dong, *J. Polym. Sci. Part A: Polym. Chem.* **2013**, *51*, 229-240.

10.1002/chem.202002525

Entry for the Table of Contents

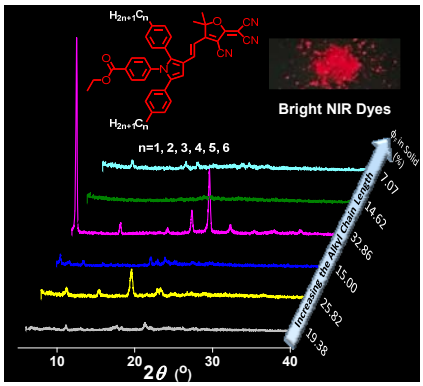

A series of multiarylpyrrole derivatives with near-infrared emission and aggregation-enhanced emission features were designed to increase the quantum yield of dyes in solid, which powder XRD data and single crystal analysis elucidated that the different lengths of alkyl chains had a significant impact on the regularity of NIR dyes when they were forced to aggregate or precipitate.